Journal of
Synchrotron Radiation

ISSN 0909-0495

Received 2 September 2005
Accepted 5 February 2006

The ID23-1 structural biology beamline at the ESRF

Didier Nurizzo,* Trevor Mairs, Matias Guijarro, Vicente Rey, Jens Meyer, Pablo Fajardo, Joel Chavanne, Jean-Claude Biasci, Sean McSweeney and Edward Mitchell*

European Synchrotron Radiation Facility, BP-220, F-38043 Grenoble CEDEX 09, France.
E-mail: nurizzo@esrf.fr, mitchell@esrf.fr

The demand for access to macromolecular crystallography synchrotron beam time continues to increase. To meet this demand the ESRF has constructed a dual station beamline using a canted undulator system as the X-ray source. The first phase of the beamline to be constructed is ID23-1, a tunable MAD-capable station with a mini-focus X-ray beam. The beamline makes use of well characterized optical elements: a channel-cut monochromator with a high-precision toroidal mirror to focus the X-ray beam. The beamline has been conceived with the aim of providing high levels of automation to create an industrial-like environment for protein crystallography. A new software suite has been developed to permit reliable easy operation for the beamline users and beamline staff. High levels of diagnostics are built in to allow rapid trouble-shooting. These developments are now being exported to the ESRF macromolecular crystallography beamline complex and have been made in a modular fashion to facilitate transportability to other synchrotrons.

Keywords: macromolecular crystallography; automation.

1. Introduction

In recent years synchrotron beam time for macromolecular crystallography (MX) has become more readily accessible. With this increased availability has come a greater demand for easy-to-use reliable beamlines (Arzt *et al.*, 2005). MX users are often unfamiliar with the operation of synchrotron beamlines. Given that many MX experiments are very similar, intuitive wizard-interface driven beamlines with high levels of automation should be possible. Indeed, the Stanford SSRL macromolecular crystallography team are conducting tests for remote-controlled user protein crystallography measurements with samples sent to the synchrotron and loaded into sample changers by beamline operators. A post-in service for academics using the Brookhaven synchrotron has already proved exceedingly popular, as have similar schemes for commercial clients at the ESRF and elsewhere. Many MX beamlines around the world are aiming for high levels of automation for both X-ray provision and sample assessment (for example, see Pohl *et al.*, 2004; Allaire *et al.*, 2005; Arzt *et al.*, 2005; Cohen *et al.*, 2005; Mairs *et al.*, 2005). In Europe the BIOXHIT initiative (http://www.bioxhit.org), funded by the European Framework Programme 6, coordinates scientists at European synchrotrons to consolidate the structure determination process with the goal of fully automated structure determination. The work on the ID23 beamlines, and more generally within the ESRF MX beamline suite, forms a core part of the BIOXHIT project.

At the ESRF the design brief of the new dedicated macromolecular crystallography complex of ID23 was to provide facilities with the highest degree of automation possible whilst enabling remote access at a later date. Furthermore, ID23-1 was to be able to handle small samples. The resulting beamline has called upon the previous experience of the ESRF MX beamlines made up of ID14 (Wakatsuki *et al.*, 1998) with four end-stations, one tunable and three fixed energy, and the fully tunable ID29 beamline. Beamline ID23 is made up of two end-stations, each operating as independently from the other as reasonably possible. The beamline is being constructed in two phases. The first-phase station, ID23-1, which is tunable, has been operational with external users since early 2004. This paper describes the progress achieved to date towards an automated user and synchrotron scientist environment with this beamline. The second end-station, ID23-2, is currently under construction and will be a micro-focus beamline dedicated to MX, and this will be the subject of a future report.

2. ID23 X-ray source

The X-ray source for ID23 is a canted undulator system made up of two undulators with a radial separation of 1.5 mrad (Fig. 1). The electron beam is deviated in the straight section of the machine reserved for undulators by means of compact iron-free permanent-magnet dipoles. This is the first time a canted system using two physically separated undulators has

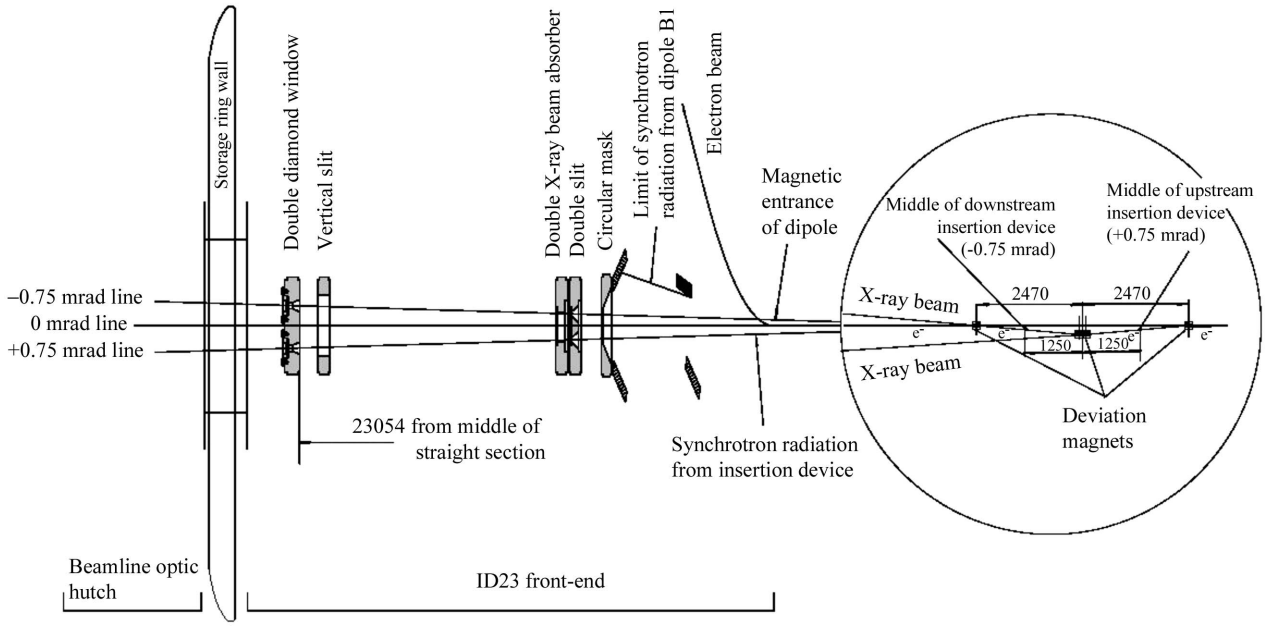

Figure 1
The canted undulator system serving X-rays to ID23-1 and ID23-2. The double diamond window at the end of the front-end is 23.054 m from the centre of the storage-ring straight section.

been inserted into the ESRF storage ring, although the technique has been used successfully at the APS (Den Hartog *et al.*, 2003; Benson *et al.*, 2004; Freeland *et al.*, 2002) and is proposed elsewhere (for example at Diamond, UK). The choice of a 1.5 mrad separation was governed by the need to separate the two beams sufficiently to pass through two distinct diamond windows on the one hand and the necessity to minimize the effort involved in modifying the front-end on the other. Future projects using canted X-ray sources at ESRF could go up to a separation of 6 mrad, but would involve a major redesign of the crotch vacuum chamber and of the front-end. The canted undulator set-up was chosen to enable the installation of two end-stations on a single straight section, whilst retaining a maximal independence of beamline operation. The adjustment of the undulator gap on ID23-1 does not affect in any way the quality of X-rays on ID23-2. However, the small separation between the two X-ray beams, some 45 mm at 30 m from the source, creates engineering design challenges. Partly to overcome the space constraints, station ID23-2 is being constructed as a fixed-energy line with a side-deflecting monochromator which allows the two X-ray beams to be very well separated after the ID23-2 monochromator (Fig. 2*a*).

The undulator installed on the ID23-1 low-β straight section is of period 35 mm and length 1.6 m and was chosen to give maximum tunability across the energy range of 5.2 keV to 20 keV, producing the output X-ray spectrum shown in Fig. 3. The front-end is based on the ESRF high-power front-end configuration (Biasci *et al.*, 2002) and is equipped with a double slit and double X-ray absorber. The diamond window chamber has been re-designed to accept two existing carbon-vapour deposited (CVD) diamond windows (0.3 mm thick, aperture of diameter 6 mm) at 23 m from the source.

3. Beamline design and automation philosophy

ID23 has been designed to provide a high level of automation and a rapidly tunable, highly stable and tightly focused X-ray beam. With the average protein crystal decreasing in size, the optical design was optimized in order to focus the X-ray beam to less than 60 µm full width at half-maximum (FWHM).

In the first instance, one may think that beamline automation is mainly dedicated to carrying out a user experiment automatically, but the definition of automation should also be extended to the beamline calibration and alignment and stability. In order to achieve the automatic alignment of the optical elements it was decided to split the beamline into virtual sections that function autonomously. The beamline was therefore separated into the following discrete parts: primary slits; monochromator and secondary slits; mirror; sample environment including sample slits, sample goniometer, detector and shutter.

When a problem is encountered it is often difficult to ascertain which of the optical devices is at the origin of the problem. Consequently, to simplify troubleshooting in the event of beam loss or instability, the beamline was planned so that each optical element section has appropriate diagnostics at the segment output, thereby giving high levels of monitoring and feedback (Fig. 2*b*). These diagnostics have, as far as technically possible, been conceived to be capable of measuring the performance to a degree of accuracy sufficient to indicate whether the element is working within specifications. However, improvements in the monitoring of beam position in terms of both precision and sampling frequency are still required.

In order to simplify instrument control and to make interaction with the beamline more efficient, a new software

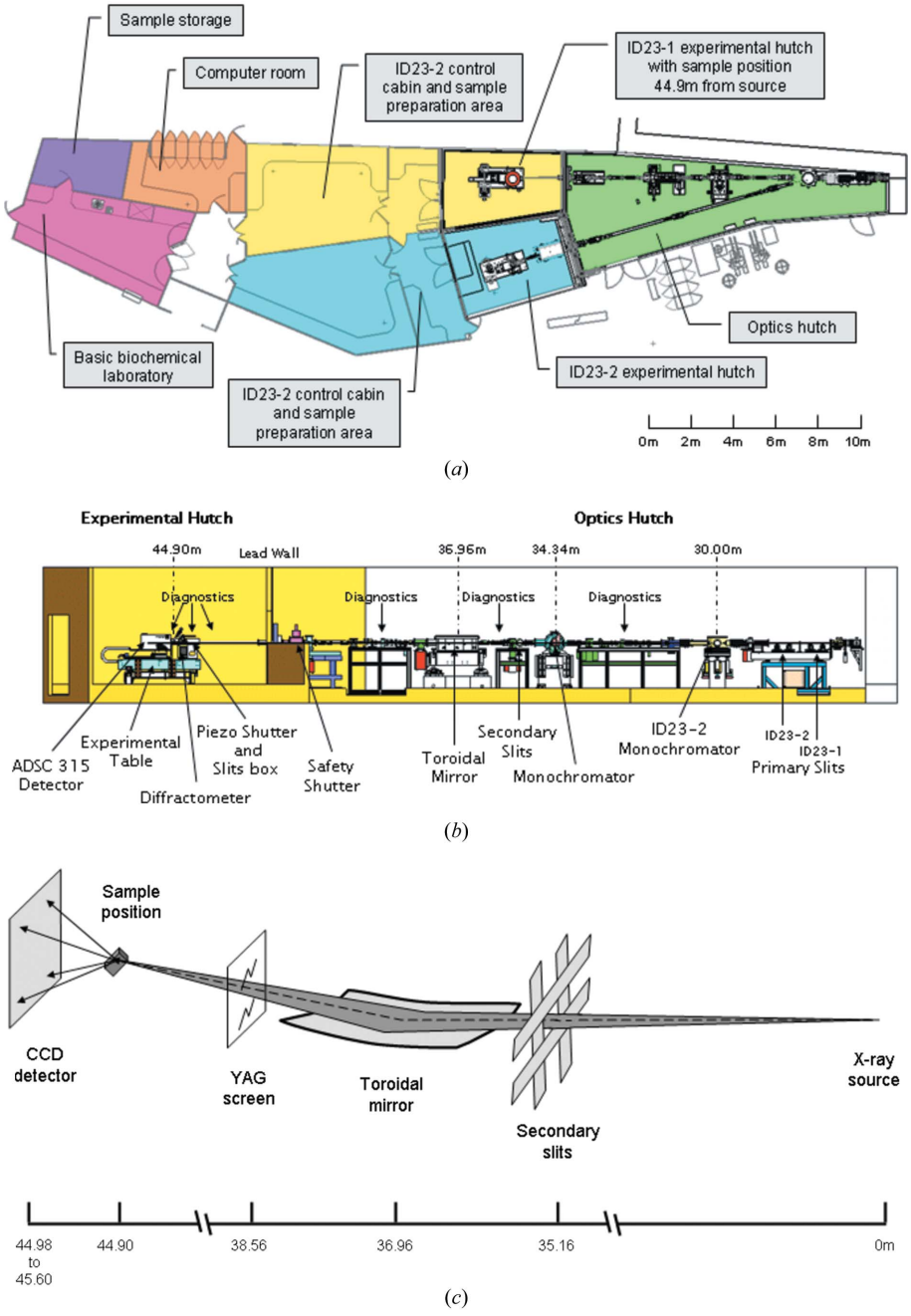

Figure 2
(*a*) Plan view of the ID23 beamline showing the optical and experimental hutches, control cabin and ancillary rooms. (*b*) Schematic showing the layout of the optical elements and experimental hutch of ID23-1 with distances relative to the centre of the straight section which is the smallest beam source point. (*c*) Schematic representation of the beamline focusing, also showing the secondary slits located just before the toroidal mirror and the YAG screen just after the mirror. An X-ray camera can be put in front of the detector for automatic beam focusing.

environment was necessary. The ethos for the control software was to distribute the control of hardware over several computers whilst retaining a principal control point on one machine where all the necessary information could be displayed and accessed. An overall synopsis of the beamline status is displayed prominently in the control cabin. It was expected that each piece of control software would be written in such a way as to make it easily distributable to the other ESRF MX beamlines with minimum reconfiguration (and possibly to other synchrotrons) and additionally to create a framework into which code from outside the ESRF could be imported easily. The following aspects had to be addressed by the software (Figs. 4*a* and 4*b*):

Automation of beam delivery to the sample, including beamline alignment, monochromator optimization and mirror focusing;

Automation of the data collection for fixed- and multiple-wavelength experiments with energy scans at the absorption edge as necessary;

Information flow and book-keeping for the high-throughput experiments;

Automatic analysis of data;

Pipeline operation with the sample changer integrated with automatic sample mounting and centring, sample screening, multi-sample collection, on-line data analysis and database recording;

Diagnostics in real time (for example, shutter synchronization data) or in a recording mode (historical database) that allows off-line analysis of events.

4. Optical design and its automation

In order to achieve the desired focal size of less than 60 µm, the demagnification ratio was set at 4.7:1, giving the layout shown in Figs. 2(*a*), 2(*b*) and 2(*c*). The key statistics of the beamline are given in Table 1. The short lever arm from mirror to sample was also expected to help increase beam stability at the sample position. In choosing the actual focusing device, consideration was given to the use of a Kirkpatrick–Baez mirror system and various other types of mirror with different sections (bent cylinder, bent cone, bent ellipse). The final decision was to use a bent cylindrical (toroidal) mirror since this is a well known and characterized system lending itself to simple and stable alignment and therefore reliable operation. Similar reasoning was behind the decision to use a channel-cut silicon monochromator. Owing to the requirements of a mini-focus beam, the mirror specifications were less than 1 µrad longitudinal slope error and 3.5 Å root-mean-square surface roughness over the 700 mm × 40 mm optically active surface of the mirror.

The beamline layout was optimized with the use of *SHADOW* (Welnak *et al.*, 1994), as implemented in the *XOP*

visual user interface (Sanchez del Rio & Dejus, 2004), which gave a theoretical focus size, including a 0.8 µrad meridional slope error modelled on the mirror, of 34 µm and 24 µm horizontal and vertical FWHM, respectively, at the sample position. The theoretical photon flux through the default 3 mm × 1 mm (horizontal by vertical) primary slit settings is 1.7×10^{13} photons s^{-1} at 13.0 keV as calculated using *SRW* (Chubar

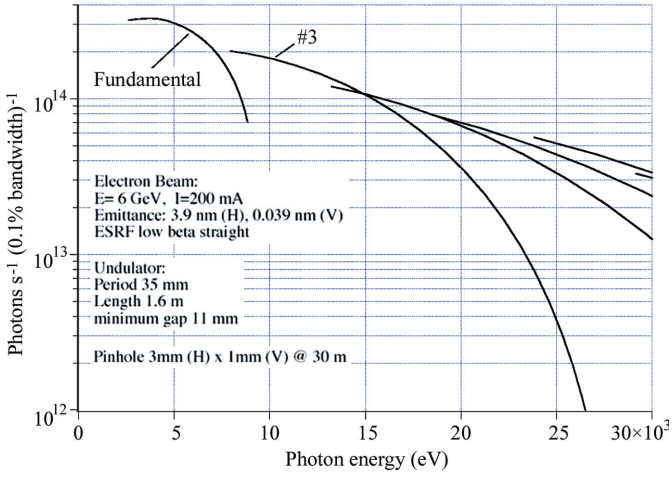

Figure 3
The output spectrum of the U35 undulator of ID23-1 shown as photons s^{-1} (0.1% bandwidth)$^{-1}$ through a 3 mm (H) × 1 mm (V) pinhole at 30 m (equivalent to the position and normal slit gaps of the primary slits) from the centre of the undulator.

Table 1
Summary of beamline ID23-1 parameters.

X-ray source	1.6 m-long 35 mm-period undulator with 11 mm minimum gap as part of a canted undulator pair serving the ID23-1 and ID23-2 end-stations. Source size (r.m.s., H × V) 59 µm × 8.3 µm. Source divergence (r.m.s., H × V) 90 µrad × 3 µrad
Monochromator (energy range)	Channel-cut double-crystal silicon [111] crystal (5.2–20 keV)
Focusing element	Toroidal mirror with Rh coating: useful area 700 mm × 40 mm; incident angle 3 mrad; sagittal radius 39.5 mm ± 0.1 mm; meridional slope error 0.8 µrad; microroughness 3.5 Å
Focusing ratio (distances)	4.7:1 (36.96 m source to mirror, 7.94 m mirror to sample position)
Third harmonic rejection at 7.0 keV	Better than 2×10^{-2}
Theoretical total flux at 13.0 keV at the sample with 200 mA stored current	1.7×10^{13} photons s^{-1}
Measured flux† at 13.0 keV at the sample with 200 mA stored current	4.5×10^{12} photons s^{-1}
Theoretical focus size at the sample position	24 µm × 34 µm (V × H) FWHM
Measured focus size at the sample position	50 µm × 60 µm (V × H) FWHM
User facilities	Local biochemistry laboratory, Linux-based graphics machines and data back-up facilities

† Using calibrated silicon photodiode.

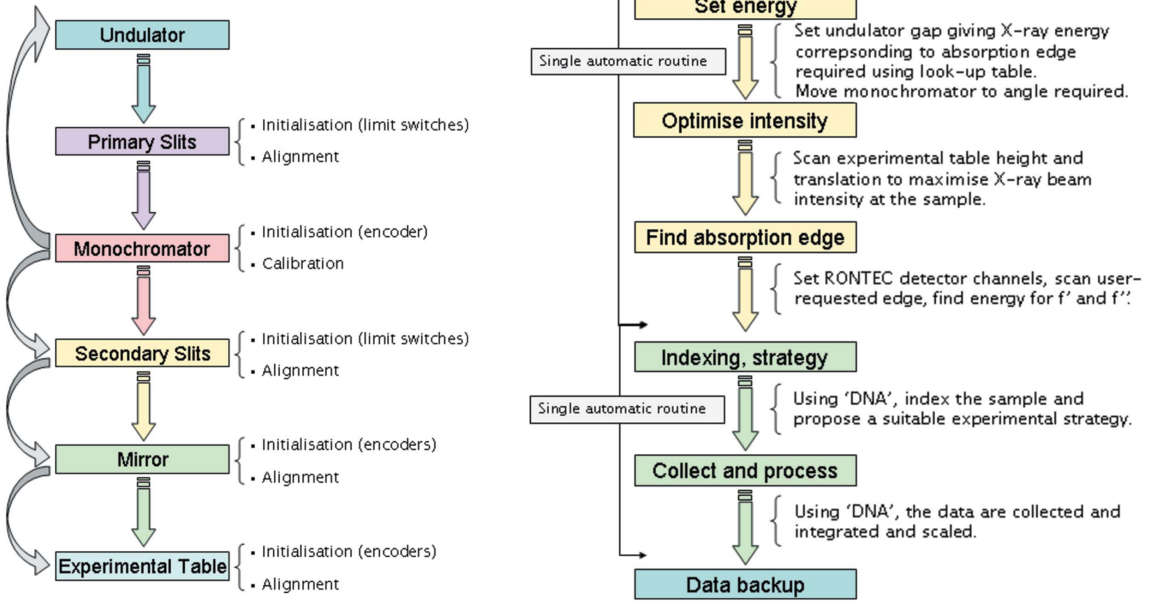

Figure 4
(*a*) Flow diagram showing the stepwise alignment of the optical elements to an optimized beamline. (*b*) Flow diagram showing the automated points along the path of a typical MAD experiment. At the ESRF, user data are backed up to a central disk and tape robot server where images are stored for up to three weeks.

& Elleaume, 1998) and taking into account the theoretical monochromator bandwidth and mirror efficiency. The measured focus size is around twice (see Table 1) that expected from the theoretical calculations and the photon flux is less than theoretically expected. These results are likely to be due in part to residual thermal slope errors on the first diffracting face of the monochromator.

4.1. Primary slits

The use of canted undulators results in severe space restrictions in the proximity of the two X-ray beams from the canted undulators. The primary slits have been designed to be narrow, in order to fit into the available space, whilst still being able to absorb a high power load of 75 W mm^{-2}. In place of using the standard four-way blade system, the ID23 devices (one for each station) consist of two solid blocks of copper mounted on separate translation tables with both vertical and transversal movement (Shu *et al.*, 1995; Marion & Zhang, 2003). The copper blocks have a gently tapered aperture through the centre, with a smallest aperture of 7 mm horizontal by 3 mm vertical, thereby distributing the absorbed white-beam heat load over a large water-cooled surface area. The beam definition is made by aligning the two apertures and then moving the blocks independently to cut the beam.

An X-ray beam viewer situated immediately downstream of the primary slits permits the beamline scientist to visualize the white beam exiting from the slits and acts as the direct visualization of the X-ray beam. The beam viewer consists of a CVD diamond foil with dimensions of 20 mm (width) $\times$ 12 mm (height) $\times$ 0.250 mm (thickness) clamped mechanically to a motorized water-cooled copper holder at 45° to the beam (Mairs *et al.*, 2005). When illuminated by X-rays, the diamond fluoresces with visible light which is captured by a black and white video camera. This progressive scan camera permits the acquisition time of the camera to be adjusted to between 20 µs and 2 s. It therefore allows acquisition of an unsaturated picture of the X-ray beam in all undulator settings.

The automatic alignment of the primary slits requires their calibration and alignment. This is accomplished by using a scattering foil of pyrocarbon which is mounted on the same motorized water-cooled copper block as the diamond foil described above. A silicon diode is used to record the scattering signal and is fitted to the vacuum pipe at 45° at the foil. A simple software algorithm sets the initial copper block positions using limit switches and then scans the slits and uses the diode reading the pyrocarbon scattering signal to align the slits so that they are centred on the white beam. A full automatic initialization, calibration and alignment takes around 5 min to complete.

4.2. Monochromator and secondary slits

ID23-1 uses a liquid-nitrogen-cooled channel-cut silicon [111] monochromator with a vertical offset. The crystal design and cooling method is an evolution of that used on ESRF beamlines ID29 and ID09 (Zhang *et al.*, 2003). An additional Compton scattering shield has been added to reduce thermal drifts owing to, for example, refills of the machine storage ring. This design was chosen because of its simplicity and easy alignment procedures. It is rotated with a Micos-controlled stepper motor with active feedback on a high-resolution Heidenhain RON806 incremental encoder (0.05 milli-degree minimum step size, corresponding to around 0.1 eV at 12.67 keV). The monochromator has a differentially pumped feedthrough, which is driven by a rotation table in air. The encoder, also in air, is rigidly connected to the feedthrough shaft and thus directly measures the Bragg angle. The disadvantage of a channel-cut monochromator is of course the intrinsic vertical movement of the beam when changing energy; however, this can be readily compensated for by adjusting the experimental table height. A scan of the vertical offset of the secondary slits is used to measure the beam vertical movement. The measured displacement is then applied to adjust the mirror height in order to maintain an optimal focus. This monochromator design has already been implemented on the ESRF MX beamline ID29 and has been shown to be robust and highly stable. With increasing interest from the user community in low-energy and particularly sulfur-SAD phasing, modifications were made to the Bragg angle limits of the ID23 device in order to increase the energy range to lower energies. The accessible energy range for ID23-1 is from 5.2 keV to 20 keV. The third harmonic rejection of the Si (111) monochromator reflection is achieved by the rhodium coating of the toroidal mirror, set at an angle of incidence of 3 mrad. Below an energy of 8.5 keV, further filtering of the third harmonic is achieved by using a pusher motor to detune the second diffracting face of the monochromator from that of the first. Tests have shown that this results in better than 0.02 harmonic rejection and an acceptable loss of around 20% on the principle beam intensity at 7.0 keV.

The position of the monochromator stepper motor is monitored by an additional absolute encoder, mounted on the driving motor axis and initialized to correspond to the beamline reference energy of 11.56276 keV (the platinum *L*-III absorption edge). The absolute encoder, model IVO GM 400, has a resolution of 8192 points per rotation over 4096 rotations giving a unique position over a 163° range. The encoder therefore allows the monochromator Bragg angle to be driven close to the reference energy without difficulty. Once there, a diode and a platinum foil are inserted into the monochromatic X-ray beam in order to record an XANES spectrum of the platinum *L*-III absorption edge. After removing the platinum foil, a spectrum of the beam intensity across the same energy range but without platinum foil is recorded to allow normalization of the absorption-edge scan. The inflexion point is automatically calculated using a purpose-written programme in Python and used to set the monochromator energy with a typical error of less than 0.1 eV.

This automatic calibration procedure allows the inexperienced beamline operator to recalibrate the monochromator. A comprehensive and automatic cross-check of the calibration can also be carried out using other metal foils held on the same actuator as the platinum foil. These foils have been chosen to

provide a spread of absorption edges across the energy range of ID23-1 (iron *K*-edge at 7.11075 keV; copper *K*-edge 8.98048 keV; platinum *L*-III, *L*-II and *L*-I 11.56276 keV, 13.27190 keV and 13.8807 keV, respectively; zirconium *K*-edge 17.99588 keV; and molybdenum *K*-edge 20.00036 keV) (Kraft *et al.*, 1996). This procedure is carried out at the start of every ESRF user scheduling period (around every two months) and/or after maintenance on the monochromator. A total of ten scans per edge are performed overnight and are analysed to calculate the energy root-mean-square deviation for each edge. In our experience this is less than 0.2 eV for all of the absorption edges scanned.

The same diode that is used for monochromator calibration also allows the calibration of the four-bladed secondary slits using a similar algorithm to that used for initializing the primary slits (§4.1).

On the actuator holding the metal foils, an additional sheet of kapton is mounted in a scattering configuration with an associated silicon pin diode (Hammamatsu) at 45° to the foil. This foil can remain in the X-ray beam and monitor the beam intensity after the secondary slits during user experiments. The foil seems to be resistant to the high photon flux and, to date, does not show significant decay over time. The same foil has been used in the X-ray beam for the last 18 months.

A final diagnostic consists of a monochromatic beam viewer, based on the white-beam viewer (§4.1), installed after the secondary slits to perform the role of ultimate monochromatic X-ray beam presence arbiter, but in this case the diamond foil has been replaced by an yttrium aluminium garnet (YAG) scintillator.

4.3. Focusing mirror

The X-ray mirror is constructed from silicon coated with rhodium and is of length 780 mm with sagittal radius 39.2 mm ± 0.1 mm and meridional radius of 4.3 km when bent optimally. The distance between the source and mirror is 36.96 m and that between the mirror and sample point is 7.94 m. The nominal angle of incidence of the mirror is 3 mrad. The ID23-1 mirror has been produced by SESO (France) to very high specification in order to attain the desired uniform X-ray beam. In tests on the unbent mirror, the ESRF Metrology Laboratory showed that the longitudinal slope error was 0.8 µrad r.m.s. and surface roughness 3.5 Å r.m.s. To date, this represents one of the finest cylindrical mirrors delivered to the ESRF. Experience has shown that beam stability at the sample position is closely correlated with the vibration levels of the mirror. Close attention has therefore been paid to reduce these effects and to minimize any amplifications of vibration levels present on the ESRF site. The mirror vacuum chamber and marble on which it is mounted are moved as a single unit in order to align the mirror to the beam. Compared with the original design, where the mirror is moved inside the chamber using vacuum feedthroughs, rather than as a solid unit with the supporting granite, the average lateral amplification over the range 0–100 Hz has been reduced from 60% to 17% and, more importantly, the principal frequencies have been shifted higher from 18 Hz to 32 Hz.

Automated beam focusing has two objectives: it must optimize the X-ray flux at the sample position and ensure a smooth beam cross section. This latter point is crucial when dealing with highly collimated beams and micrometre-sized crystals. The ID23-1 automatic-focusing procedure performs an alignment of the mirror to the beam followed by an optimization of the focal spot at the sample or at the detector front face. The first stage of the alignment uses the same philosophy as that implemented for the monochromator: five absolute encoders are able to bring the mirror to a flat initial reference position. From this initial position the mirror is tilted to 3 mrad. An optical camera visualizes the fluorescence generated by the X-ray beam passing through a YAG screen positioned after the mirror and the signal intensity and the centre of gravity of the beam are calculated from this camera image. A scan of the intensity *versus* mirror height or horizontal translation then allows the geometrical centre of the mirror to be aligned to the incoming X-ray beam. This procedure, using an initial absolute position of the mirror, relies on the long-term positional stability of the X-ray beam produced by the machine. To date, following 18 months of operation, it has not been necessary to reset the reference position of the mirror.

This first stage of the mirror alignment is followed by a more complex analysis of the X-ray beam focus. A wavefront analysis method has been developed at the ESRF (Hignette *et al.*, unpublished) to automatically pre-align and align X-ray mirrors by taking advantage of secondary slits placed between the monochromator and mirror. This method has been employed successfully on beamlines using toroidal and Kirkpatrick–Baez mirror systems and sagittally focusing monochromators. The rotations (yaw and incident angle) and bender tension are optimized using a camera mounted on an actuator in front of the X-ray diffraction detector in the experimental hutch and therefore at or near the sample position. The changes in X-ray beam position at the focal point are measured during a scan of the slits across the beam incident to the mirror. This is carried out for five different orientations of the mirror and a matrix is calculated from which the optimal mirror orientation is derived and then driven to.

The beamline staff make use of the procedures above to align the beamline optics ready for users. Most of the algorithms are, however, also coded into the user-level software for automatic energy changes and optimization of the X-ray beam.

4.4. Beamline diagnostics

Once all beamline elements are in their correct alignment it is essential that their positions are continually monitored, stored and compared with those corresponding to an optimum alignment of the beamline. On ID23, diagnostic data are recorded continuously using the ESRF storage-ring database, keeping track of machine performance parameters. This machine historical database (HDB) has been extended to

allow the deposition of beamline data, which allows one to trace and correlate beamline events in time. All parameters, including the motor positions, temperature of optical components, beam positions and beam intensity, vacuum, machine intensity and state are archived centrally through a store server operating in the background. The configuration of the HDB allows different polling periods for each signal to be defined. This also enables recording to be triggered in an event-driven mode where storing actions commence on value changes above pre-defined levels. Automatic on-line interrogation of the HDB coupled with feedback to the beamline control software should then allow one to maintain a beamline in its optimal configuration. A dedicated application allows interactive queries to the HDB and a display of the recorded signals. Off-line interrogation of the HDB may allow elucidation of reasons for sudden decreases in diffraction data quality as well as identification of beamline components most prone to failure. The HDB can also be a source of information to find suitable criteria for the development of automatic and decision-taking algorithms by analysing data stored over a long period of time.

5. User experimental equipment and environment

The ID23-1 end-station has benefited from the knowledge acquired on MX beamlines at the ESRF and has built upon the developments of the sample changer (see http://www.embl-grenoble.fr/groups/instr and Cipriani *et al.*, 2006) and high-precision microdiffractometer (Perrakis *et al.*, 1999) to create a compact and ergonomic user environment. A number of automatic routines have been put in place to allow a standard multi-wavelength anomalous diffraction (MAD) experiment to proceed with little user intervention (Fig. 4*b*).

Macromolecular crystallographers typically use the beamline for short periods: a standard user visit at the ESRF consists of many experiments over a 24 h period. The layout of the control cabin has been designed in order to keep the area quiet and easy to use: the computer boxes have been moved to a computer and hardware room with the screens and keyboards making use of remote display and function through a keyboard–video–mouse system. The control cabin is separated from the experimental hutch by a basic sample preparation area fitted with a bench, temperature-controlled cupboard and microscope.

5.1. Experimental hutch

The experimental hutch is relatively small ($\sim$10 m^2) to make air conditioning and humidity control practical. To avoid vibration, all sources of vibrations have been moved outside of the experimental hutch. The experimental table is a 2200 mm $\times$ 960 mm $\times$ 280 mm block of granite mounted on three vertical legs plus two horizontal translation stages allowing a total of five degrees of freedom. The table supports the slit box, the diffractometer and the CCD-based detector, all of which are bolted firmly to the table (Fig. 5).

The temperature of the sample is controlled using a Cryostream 700 series from Oxford Cryosystems (the nitrogen dewar is refilled automatically) mounted on a pneumatic actuator with a 1.5 cm translation. This translation moves the nozzle away from the crystal to allow access for the sample changer or for a user to mount a crystal. It is also possible to remotely insert a cryoshutter installed on the cryostream nozzle in order to anneal a crystal with precise timings.

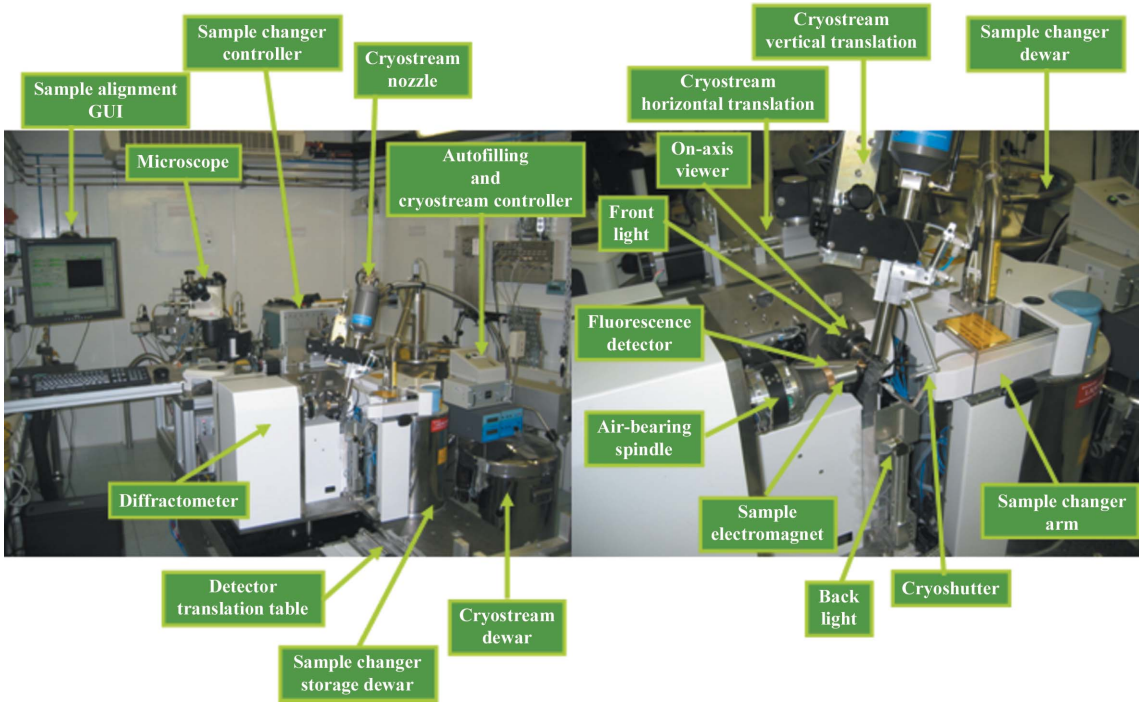

Figure 5
Left: photograph of the ID23-1 experimental hutch showing the sample environment and surrounding equipment. Right: a close view of the sample environment.

The visualization of the sample uses an on-axis camera as first used on the microdiffractometer (Perrakis *et al.*, 1999). An automatic procedure, based on edge detection, has been implemented that allows samples to be automatically focused in the sample in the field of the CCD camera.

The diffractometer itself is based on an air-bearing spindle axis with a sphere of confusion of less than 2 μm diameter (Perrakis *et al.*, 1999). This spindle is mounted on an *xyz* translation table and fitted with two motorized translation tables for aligning the crystal to the X-ray beam. With the arrival of sample changers, one of the most difficult problems concerning automation is the automatic alignment of samples in the beam. There are currently three methods for doing this. The first, and most simple, is a computer-assisted method where the user identifies the sample on the graphical interface at three different spindle positions (typically 0, 90 and 180°). The software can then determine the translations necessary to place the crystal centre on the rotation axis and to align the sample. The second method, using image analysis from the on-axis camera, automatically identifies the loop holding the sample and aligns it following the same algorithm with the user subsequently aligning the sample itself as above. A third method, with much more complex image analysis, allows fully automatic sample aligning and centring (Andrey *et al.*, 2004). It has the drawback of not yet being 100% reliable and being slower, with the whole sequence of movements and analysis taking currently 2 min. Typically the first method is the fastest and more reliable when users are present. The third method is planned to be used for multi-sample unattended screening and data collection. Recent crystal centring tests have been carried out on the beamline using a laser. This method is still under development but has shown exciting initial results. It will shortly be implemented on the beamline and be available to users.

By placing a YAG screen at the sample position, the X-ray beam shape can be directly visualized and the centre of mass calculated. Knowing the centre of the beam and the calibration of the camera, it is simple to calculate the horizontal and vertical translations to apply to the experimental hutch table and slit systems for moving the beam centre onto the centre of rotation. This procedure has been fully implemented and it is accessible directly from the user software interface.

The quality of the rotation axis and the synchronization of the fast shutter with the rotation axis is important. The fast shutter is based on a piezo design (see http://www.embl-grenoble.fr/groups/instr) with a 400 μm horizontal aperture, an opening and closing time of less than 3 ms and fitted with strain gauges for status monitoring. These components have often been blamed for the poor quality of the data in the past and are amongst the beamline components undergoing the most cycles (Flot *et al.*, 2006). It is, therefore, imperative that the quality of the synchronization (spindle position *versus* opening/closing of the shutter) is monitored continuously during the experiment. On ID23-1 several signals are recorded systematically during each image of the data collection: the encoder position of the rotation axis, the status of the command open/close shutter, the actual status of the shutter as read from the strain gauges and the X-ray beam intensity before and after the shutter. These signals are entered into a multi-purpose unit for synchronization, sequencing and triggering (MUSST) card custom-built at the ESRF. The frequency of sampling by the card is adjustable and is calculated before each image as a function of the acquisition time of the image. This diagnostic is currently stored in a data file and saved automatically in the user directory where the diffraction images are written. In the future it is planned to store this information in the historical database.

The beamline was originally equipped with a MAR 225 detector. This has been changed to a Quantum 315R from Area Detector Systems Corp during November 2005. The sample-to-detector distance can vary from 55 mm to a maximum 700 mm corresponding to a maximum detectable resolution of 0.54 Å for the circle inscribed in the ADSC detector square face with 20.0 keV energy X-rays.

5.2. Adjoining user environment and data back-up

Beamline users occasionally bring unfrozen crystals to the beamlines; therefore a biochemical laboratory next to the control cabins and shared between ID23-1 and ID23-2 has been constructed as part of the beamline. It includes the standard equipment for the preparation of heavy-atom derivatives and also an Oxford Xenon cell for xenon derivatization. Space adjoining this laboratory has been dedicated to the ESRF MXpress industrial service in order to store cryogenically cooled samples.

The beamline is currently able to produce up to 40 images a minute. In order to handle this data throughput, gigabit Ethernet links are provided between the ESRF central storage disks and the Linux and Windows CCD control and data back-up computers at the beamline. These computers, which also have high-quality graphics cards for visualization of structures, are installed in the control cabin allowing the users to back up the data following the data collection but without disturbing the data processing. Several Linux computers are also accessible to users in a dedicated back-up room near to the beamline.

Even before the recent sample changer installation, the influence of which is not yet fully known, users have been able to collect huge numbers of images in a 24 h period. Over the last 12 months, just over half a million images have been taken, with the peak daily rate representing 8000 images, corresponding to 140 GB of data from the original MAR 225 detector made up of 28 data sets and 35 crystal diffraction tests.

6. Software and control environment

In order to meet the beamline requirements outlined earlier and to make the automation described above reliable and easy to use, the beamline control environment and the graphical interfaces offered to beamline staff and users have been redesigned. The result is the software environment called *exes*.

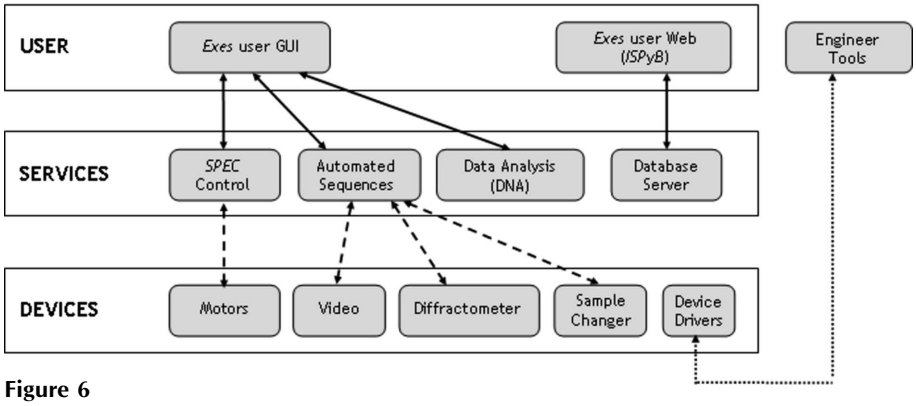

Figure 6
Schematic of the three-level approach to the software control environment. The user (which may include beamline staff) interacts principally with the highest level of software. If necessary the mid-level sequencing-type software can be accessed directly, but this is only usual for troubleshooting by the beamline staff. Individual devices, such as the motors, video acquisition and sample changer, are controlled by the mid-level software working on Linux-based PCs.

The *exes* software controlling the ID23 optics and experiments is based on the classic three-level approach (Fig. 6) used at all the ESRF beamlines. This includes:

User-level software: user interfaces in the form of graphical applications for control or web-based applications for local and remote access to information.

Sequencer software and servers: the features of the hardware are modelled as abstract classes (motor, counter, detector *etc.*). These features are used by macro languages to define the experiment and data collection sequences in an easy and flexible way where all references to the hardware details (private communication protocols, specific configuration, and network access) have been removed.

Front-end software: a low-level layer devoted to the instruments. At this level, software is distributed over different beamline computers since performance and specialization are crucial. Programs at this level are mainly written in C/C++ and run on either Linux or Windows platforms depending solely on the availability and convenience of the device drivers. Remote access is obtained through an ESRF-developed communication layer abstraction called *Taco* (see http://www.esrf.fr/taco/ for further information).

6.1. User interface

The existing graphical interface for users needed special attention. The final implementation choice is based on the Python programming language and Qt graphics library. The Python to Qt binding (PyQt) provides high-quality graphics and good performance. The Python programming language is the language of choice for this project owing to its flexibility and integrative capabilities. All these features allow optimal and modular programming where the final application is the result of joining together component 'bricks', each of which has a specific function. This approach should ease the evolution of the application to integrate new instruments or experimental methods. The software configuration of the hardware components corresponds to the modularity and flexibility of the application through the use of an XML-based configuration database. The XML language provides a structured organization of parameters and links between the different hardware components.

A critical part of *exes* is an ergonomic user interface for the users and beamline staff. This interface is based on an underlying framework of four components:

(i) A hardware repository that centralizes the access to sequencers and polling devices. Hardware items are described as XML files.

(ii) A collection of modules for hardware objects that model the behaviour of the different beamline components. The hardware repository serves instances of these objects.

(iii) A library of graphical bricks representing the access to instruments, beamline procedures.

(iv) A graphical application framework that constitutes the backbone of the final application.

This model allows different views of the beamline to be created as separate instances of the same application. In this way three different instances run on ID23-1. One is used during experiments. This simple and intuitive application guides the user through the most standard beamline operations (Fig. 7*a*). The second one is dedicated to expert users where full access is available to all the beamline components (Fig. 7*b*). A third instance runs permanently in a separate monitor showing operating and diagnostics information in a purely display mode with no control possibilities (Fig. 7*c*). These developments are currently being spread to the other ESRF MX beamlines at the same time that the automatic sample changers are being installed.

6.2. Information tracking and book-keeping

High-throughput experiments require a systematic approach to the handling of sample information. The ISPyB project is a two-fold development including a database design specific for MX experiments and an online web interface, both of which make use of data models for macromolecular crystallography experiments (see http://www.e-htpx.ac.uk). ISPyB obtains information from the ESRF user office database containing proposal information and safety authorization. Users can also introduce information in advance of the experiment about dewars and samples that can be later used to control the sample changer and help make decisions during data collection. The *exes* beamline control module records information (such as data collection parameters) to the ISPyB database produced during the experiment. Information generated during the data analysis with *DNA* (Leslie *et al.*, 2002), which is installed on ID23-1, is also linked to the samples through this database. *DNA* is a project that integrates all the data analysis software and suggests data collection strategies. *DNA* can then call the beamline control

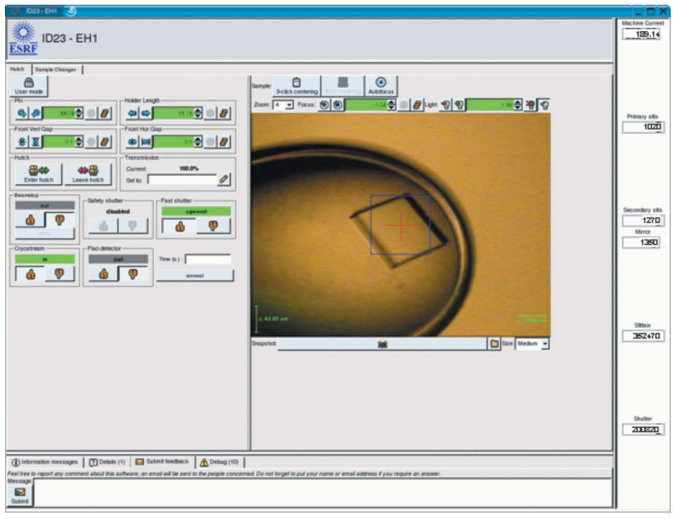

(*a*)

(*b*)

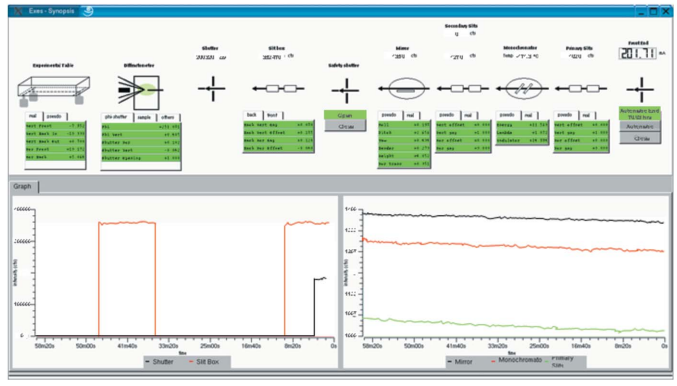

(*c*)

Figure 7
(*a*) The user graphical control interface for *exes*. The interface has separate panes for sample alignment and basic hutch control (shown above), for sample changer control and for data collection. Beamline staff and experienced users can access higher levels of functionality through a password-protected expert interface. The motor controls change colour to facilitate use: green = available, yellow = moving, red = unavailable or fault state. The lower part of the interface is reserved for log messages and information from the storage-ring operators. (*b*) The overall *exes* graphical control panel with full access to all the beamline motors and devices. This panel is typically used by local contacts and the beamline staff for troubleshooting and non-standard operations. The motor controls change colour as for the user GUI. Intensity measurements from the beamline diagnostics and machine status are shown in the top of the window. (*c*) The beamline synopsis view on display in the ID23-1 control cabin. Beam intensities are continuously tracked in the two graphs at different points along the beamline. The upper part of the screen shows motor positions and temperatures of components. The synthesis will be refined as experience is gained of important parameters and information.

module and trigger the experiment. The *DNA* software package is now available for download (see http//:www.dna.ac.uk).

Data collection, recorded in the ISPyB database, and data analysis are integrated together during the operation of the sample changer. It is possible today to run screening experiments automatically on a series of samples mounted in a sample changer. Information about the samples is taken from the database, the data collection sequence is run and data analysis is performed in parallel. The results are automatically sent back to the database and are available in the ISPyB web interface. The first ESRF pipeline experiment took place in March 2005 on beamline ID14-3. It will become a standard way of operation once all of the ESRF MX beamlines are provided with automatic sample changers. During the March 2005 experiment, one series of 17 samples was mounted, collected and analysed without any operator intervention.

7. Low-energy phasing

The use of small anomalous diffraction signals has been described (Wang, 1985). Recent developments to enable their day-to-day use in determining phases for protein structures (for examples see Liu *et al.*, 2000; Gordon *et al.*, 2001; Micossi *et al.*, 2002; and a review by Ramagopal *et al.*, 2003) show the feasibility of these experiments. The design of ID23-1 was made with low-energy single-wavelength anomalous diffraction (SAD) techniques in mind. The number of windows along the X-ray path has been reduced to a minimum and all diagnostic scattering diodes present in the X-ray beam can be moved out in order to reduce beam absorption. An initial test of sulfur SAD phasing on ID23-1 using crystals of a hypothetical protein from *Deinococcus radiodurans* was successful. The crystal belongs to the hexagonal space group $P6_1$ with $a = b = 81.3$ Å, $c = 70.4$ Å with two molecules in the asymmetric unit. A data set of 720 images was collected using 7.0 keV X-rays and integrated and reduced using *MOSFLM* (Leslie, 1992) and *SCALA* from the CCP4 program suite (Collaborative Computational Project, Number 4, 1994), giving the statistics summarized in Table 2. The sulfur substructure was determined using *SHELXD* (Schneider & Sheldrick, 2002) with data truncated to between 25 Å and 4 Å. A total of six major sites out of eight potential ones were clearly identified and used as input to *SHARP* (de la Fortelle & Bricogne, 1997) for phase refinement and density improvement giving the

Table 2
Data collection and phasing statistics for a sulfur SAD data collection on ID23-1.

Space group	$P6_1$
Wavelength in Å (energy in keV)	1.771 (7.000)
Number of images	720
Oscillation (°)/exposure time (s)/number of pass	1/1/1
Resolution in Å (highest-resolution shell)	25.0–2.0 (2.11–2.00)
Number of unique reflections	17967 (2638)
Completeness/anomalous completeness (%)	99.9/99.9
$I/\sigma I$	6.7 (3.1)
Multiplicity/anomalous multiplicity	42.9 (41.5)/21.9 (21.1)
$R_{\rm merge}$ (%)	8.1 (23.6)
Mid-slope of anomalous normal probability	1.203
Phasing power and figure of merit before solvent flattening	0.891 and 0.358

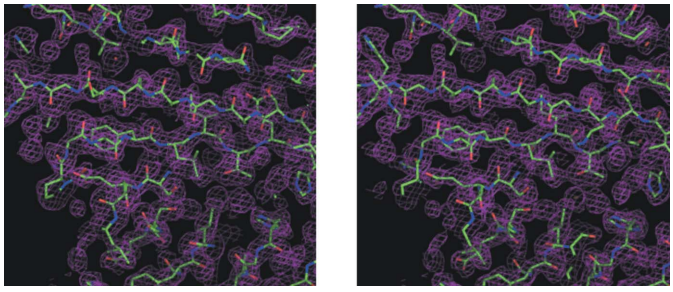

Figure 8
Stereo diagram of the electron density map contoured at 1σ after phasing and solvent flattening as performed by *SHARP*. The structure shown is the coordinates as built by *ARP*/*wARP*.

electron density map shown in Fig. 8. *ARP*/*wARP* (Morris *et al.*, 2002) was able to build 202 residues out of a total of 204 that are visible in the final model.

8. Future perspectives

The evolution of the ID23 beamlines is continuing. The development is an effort of the whole MX group plus the software and hardware teams at the ESRF. As the ID23 environment is proven, the appropriate sections will be (and are being) moved to the other MX facilities at the ESRF. In turn, new developments and improved code from the MX beamlines are being re-imported to ID23. This will provide a uniform environment, easier for both the synchrotron staff and beamline users to manage both day-to-day and in the longer term. Collaboration has been crucial to the development of the ID23 beamline and a number of the software packages have been written specifically with ease of export to other beamlines and other facilities in mind:

(i) The sample-centring algorithms have been developed at the EMBL Grenoble Outstation and integrated later within the ESRF software environment.

(ii) ISPyB is being developed following the initial PXweb project and around the data model defined after agreement between many European participants in the MX community. The UK-based eHTPX initiative (http://www.e-htpx.ac.uk) has been particularly effective in pushing forward data models. A first installation of ISPyB has already been made at Daresbury SRS.

(iii) The *exes* user interfaces are developed in an extremely modular way so that they may be adapted for use at other facilities.

(iv) Software for beam delivery automation has been the object of a workshop organized at the ESRF and even if, by its very nature, it is beamline specific, algorithms and methods are being exchanged.

(v) DNA is the very example of a successful multi-institutional development where developers contribute from ten different institutes.

This collaboration and modularity should make it simpler for the developments to be translated to other facilities around the world and for improvements and outside developments to be subsequently re-imported to the ESRF.

The authors would like to gratefully acknowledge the Macromolecular Crystallography and support groups of the ESRF and particularly the technicians and engineers. Without their active participation, ideas and advice, the construction and development of beamline ID23-1 would have been impossible. The construction of ID23-1 was supported by the FP6 EU CISB grant under contract number 01195-RICN.

References

Allaire, M., Berntson, A., Jain, A., Jakoncic, J., Kao, C. C., Siddons, D. P., So, I., Venkatagiriyappa, V., Yin, Z. & Stojanoff, V. (2005). *Synchrotron Rad. News*, **18**, 23–27.
Andrey, P., Lavault, B., Cipriani, F. & Maurin, Y. (2004). *J. Appl. Cryst.* **37**, 265–269.
Arzt, S. *et al.* (2005). *Prog. Biophys. Mol. Biol.* **89**, 124–152.
Benson, C., Trakhtenberg, E., Jaski, Y., Brajuskovic, B., Collins, J., Den Hartog, P., Erdmann, M., Rossi, E., Schmidt, O., Toter, W. & Wiemerslage, G. (2004). *AIP Conf. Proc.* **705**, 466–469.
Biasci, J.-C., Plan, B. & Zhang, L. (2002). *J. Synchrotron Rad.* **9**, 44–46.
Chubar, O. & Elleaume, P. (1998). *Proceedings of the Sixth European Particle Acclerator Conference (EPAC98)*, pp. 1177–1179. Bristol: IOP Publishing.
Cipriani, F. *et al.* (2006). *Acta Cryst. D*. Submitted.
Cohen, A. E., McPhillips, S. E., Song, J. & Miller, M. D. (2005). *Synchrotron Rad. News*, **18**, 28–35.
Collaborative Computational Project, Number 4 (1994). *Acta Cryst.* D**50**, 760–763.
Den Hartog, P., Decker, G. A. & Emery, L. J. (2003). *Proceedings of the 2003 Particle Accelerator Conference*, edited by J. Chew, P. Lucas and S. Webber, pp. 833–835. Piscataway, NJ: IEEE.
Flot, D., Gordon, E. J., Hall, R. R., Leonard, G. A., McCarthy, A., McCarthy, J., McSweeney, S., Mitchell, E., Nurizzo, D., Ravelli, R. G. B. & Shepard, W. (2006). *Acta Cryst.* D**62**, 65–71.
Fortelle, E. de la & Bricogne, G. (1997). *Methods Enzymol.* **276**, 472–494.
Freeland, J. W., Lang, J. C., Srajer, G., Winarski, R., Shu, D. & Mills, D. M. (2002). *Rev. Sci. Instrum.* **73**, 1408–1410.
Gordon, E. J., Leonard, G. A., McSweeney, S. & Zagalsky, P. F. (2001). *Acta Cryst.* D**57**, 1230–1237.
Kraft, S., Stümpel, J., Becker, P. & Kuetgens, U. (1996). *Rev. Sci. Instrum.* **67**, 681–687.

Leslie, A. G. W. (1992). Joint CCP4 + ESF-EAMCB Newsletter on Protein Crystallography, No. 26.
Leslie, A. G. W., Powell, H. R., Winter, G., Svensson, O., Spruce, D., McSweeney, S., Love, D., Kinder, S., Duke, E. & Nave, C. (2002). *Acta Cryst.* D**58**, 1924–1928.
Liu, Z.-J., Vysotski, E. S., Chen, C.-J., Rose, J. P., Lee, J. & Wang, B. C. (2000). *Protein Sci.* **9**, 2085–2093.
Mairs, T., Fajardo, P., Meyer, J., Mitchell, E., Nurizzo, D., Rey-Bakaikoa, V., Shepard, W. & Svensson, O. (2005). *Proceedings of the Third International Workshop on Mechanical Engineering Design of Synchrotron Radiation Equipment and Instrumentation (MEDSI 2004).* ESRF, Grenoble, France.
Marion, P. & Zhang, L. (2003). *AIP Conf. Proc.* **705**, 320–323.
Micossi, E., Hunter, W. N. & Leonard, G. A. (2002). *Acta Cryst.* D**58**, 21–28.
Morris, R. J., Perrakis, A. & Lamzin, V. S. (2002). *Acta Cryst.* D**58**, 968–975.
Perrakis, A., Cipriani, F., Castagna, J. C., Claustre, L., Burghammer, M., Riekel, C. & Cusack, S. (1999). *Acta Cryst.* D**55**, 1765–1770.
Pohl, E., Ristau, U., Gehrmann, T., Jahn, D., Robrahm, B., Malthan, D., Dobler, H. & Hermes, C. (2004). *J. Synchrotron Rad.* **11**, 372–377.
Ramagopal, U. A., Dauter, M. & Dauter, Z. (2003). *Acta Cryst.* D**59**, 1020–1027.
Sanchez del Rio, M. & Dejus, R.J. (2004). *Proc. SPIE*, **5536**, 171–174.
Schneider, T. R. & Sheldrick, G. M. (2002). *Acta Cryst.* D**58**, 1772–1779.
Shu, D., Brite, C., Nian, T., Yun, W., Haeffner, D. R., Alp, E. E., Ryding, D., Collins, J., Li, Y. & Kuzay, T. M. (1995). *Rev. Sci. Instrum.* **66**, 1789–1791.
Wakatsuki, S., Belrhali, H., Mitchell, E. P., Burmeister, W. P., McSweeney, S. M., Kahn, R., Bourgeois, D., Yao, M., Tomizaki, T. & Theveneau, P. (1998). *J. Synchrotron Rad.* **5**, 215–221.
Wang, B. C. (1985). *Methods Enzymol.* B**115**, 90–112.
Welnak, C., Chen, G. J. & Cerrina, F. (1994). *Nucl. Instrum. Methods A*, **347**, 344–347.
Zhang, L., Lee, W. K., Wulff, M. & Eybert, M. (2003). *J. Synchrotron Rad.* **10**, 313–319.